Supporting online information:

This document provides

A) Further data on boundary layer meteorology transport simulations that aim to describe the VOC dilution during the transport from the forest edge towards the central measurement point at the hill top.

B) Calculation of OH and HO_2

C) Correlation of $J(O^1D)$ and OH

D) Mean daily intercomparison of individual hypotheses (A), (B) and (C)

E) Mean daily intercomparison of stepwise transfer from (C) to (B)

F) Individual linear regression of compounds with the particle formation rate J_3

A) Boundary layer meteorology transport simulations

1. Domain resolution

The surface was resolved in 5 m steps based on the ALKIS-dataset provided by the Hessian local agency for surface management and geo information (HLBG). The structure is displayed in Figure S1.

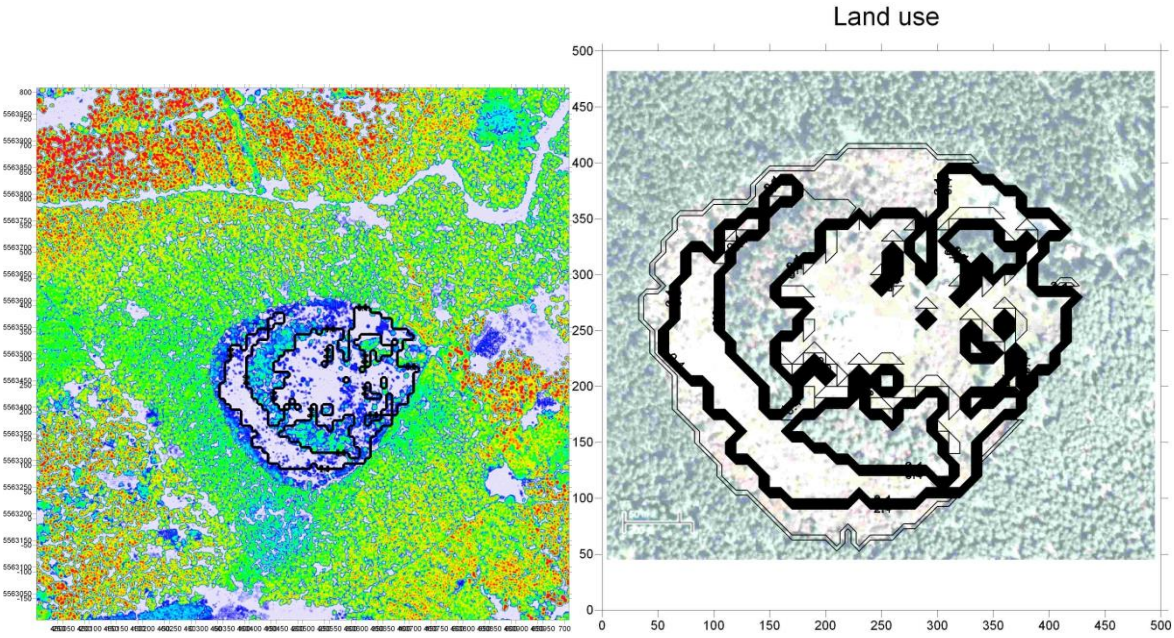

Figure S1. ALKIS-dataset (left) of surface height and distribution of vegetation. Cyan and blue colours indicate the presence of trees, while white is used for grass or bare soil. The surrounding forest at lower altitudes is displayed in greenish colours. The model resolved input for dilution calculation analysis is shown on the right.

The simulations were performed for the four major wind directions North, East, South and West. Therefore a reasonable inert trace gas emission was assumed (CO_2) and its dilution quantified at standard conditions (wind speed). Subsequently the results were normalized with respect to ambient mixing ratios i.e. a value of unity was obtained at the forest edge declining towards the hill top in wind direction. Since most of the measurements were performed at a height of 4 m above soil, this height was taken as a reference height. The corresponding results are provided in Figures S2-S5.

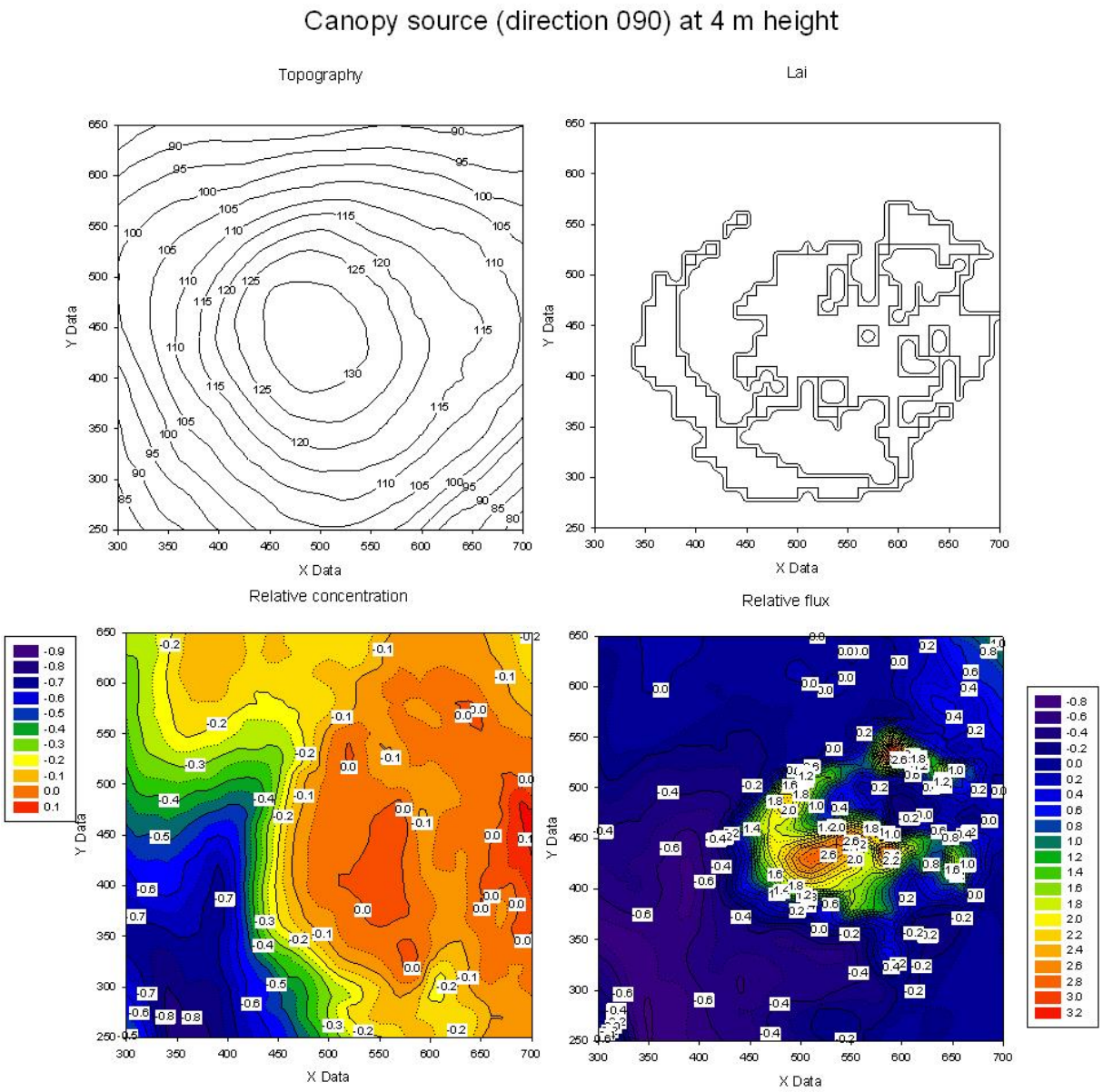

Figure S2. Dilution calculations for westward wind direction (90°).

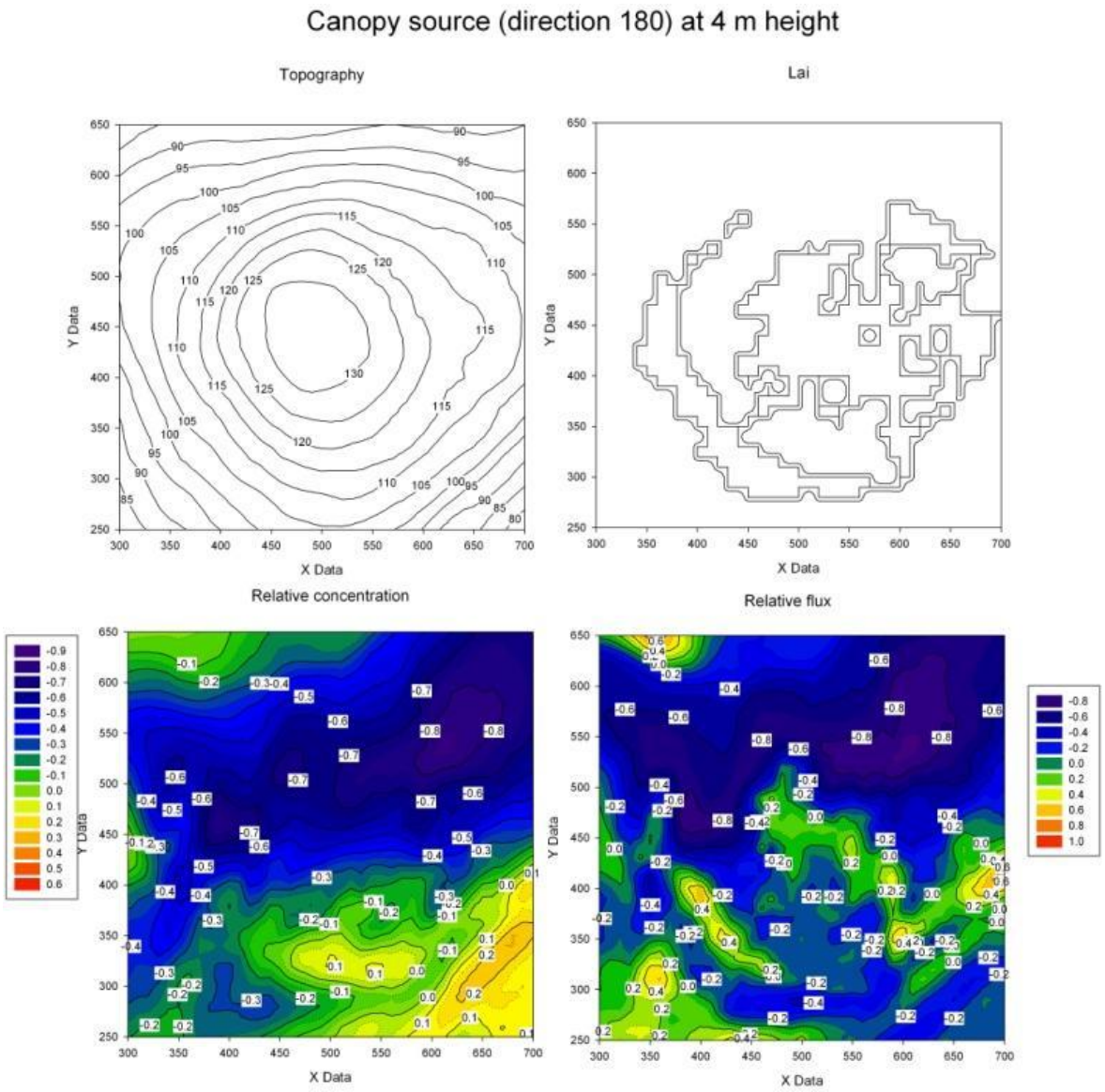

Figure S3. Dilution calculations for northward wind direction (180°).

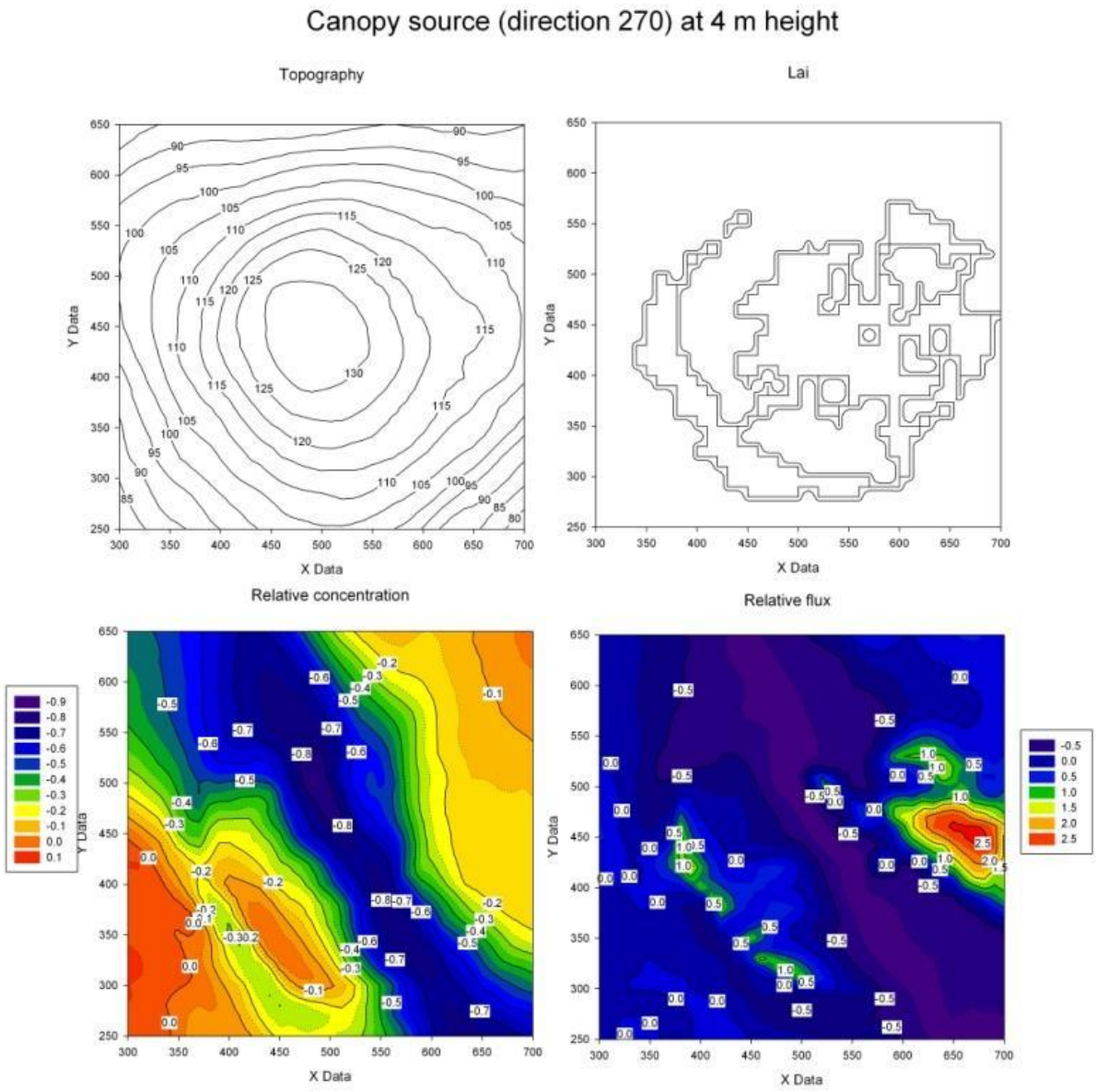

Figure S4. Dilution calculations for eastward wind direction (270°).

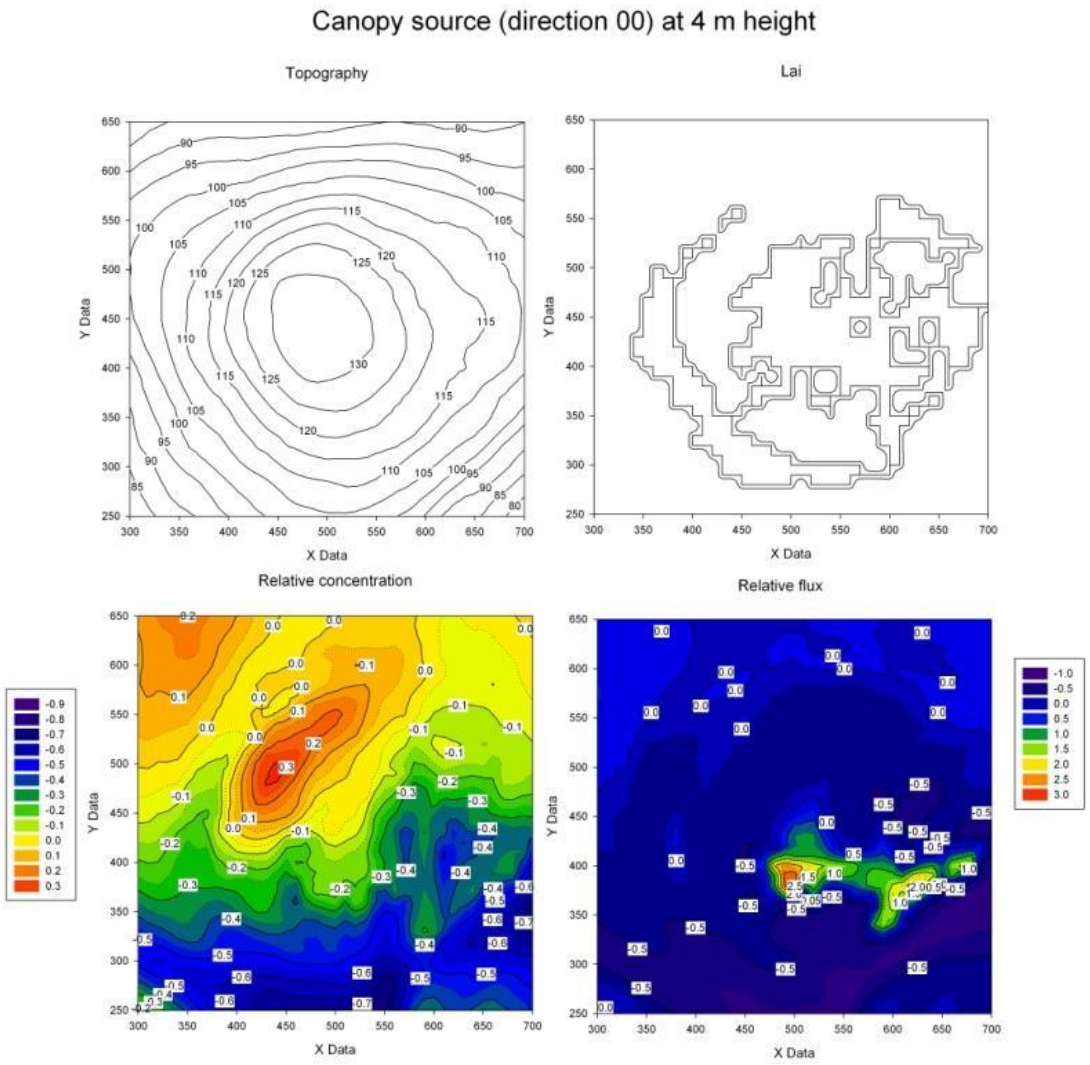

Figure S5. Dilution calculations for Southward wind direction (0°).

As an approximation these values are then used for linear interpolation in between.

2. Transport time

The transport time was derived applying the closest point of the forest opposite to the wind direction from e.g. the hill top and followed stepwise backward applying the mean wind speed measured by HLUG halfway in between edge and the hill top centre. Since the corresponding place was calculated by the simulation too, the transport time results to

$$transport\ time = \frac{distance(m)}{v_{winddir}(HLUG)}$$

and the reduction to

$$reduction = reduction(sim) \cdot \frac{v_{winddir}(sim)}{v_{winddir}(HLUG)}.$$

This can be used to gain a dilution constant k_{dil} *that has the unit of* s^{-1}:

$$k_{dil}(t) = -\frac{\log(reduction)}{transport\ time}.$$

The constant is further used in a kinetic sense similar to chemical reactions that is an exponential decline with increasing transport time and in this way chemical losses can be considered, too:

$$[X](t) = [X](t=0) \cdot \exp\left(-\left(k_{dil} + k_X^Y [Y]\right) \cdot tranport\ time\right)$$

In here k_X^Y abbreviates a reaction rate constant of compound X with compound Y and [ ] expresses a chemical molecular concentration.

B) Calculation of OH and HO_2

Based on the approach (1) of Rohrer & Berresheim (2006)

The calculation of OH and HO_2 is based on the generalized reaction scheme of Rohrer & Berresheim (2006) extended by the nitrogen compounds affecting OH in a significant way, i.e. HONO, HNO_3, HO_2NO_2. The same equations (1) – (14) as provided by Rohrer & Berresheim (2006) are used. In Eq. (3) the OH reactions with HONO, HNO_3, HO_2NO_2 and N_2O_5 are included as OH sink terms too and the lifetime of the oxidation with respect to the nitrogen compounds is abbreviated by τ_{Nit}. However the simplifications are made only where applicable:

- ↓ On the contrary to Rohrer & Berresheim (2006) the sink term of OH by NO_2 is not smaller than $\tau_{HC,N}^{-1}$ but in the same range or even above.
- ✓ $[HO_2]\cdot k_{HO2+NO}$ is small compared to $[O_3]\cdot k_{NO+O3}$.

If these modifications are applied the following α, F_J and τ_{HC} values are calculated:

$\alpha = 0.08\pm0.02$

$F_J = 1.4\pm0.6$

$\tau_{HC} = 2.1\pm0.8\ s^{-1}$

While fine for Jungfraujoch the simplified equation no. 18 of Rohrer & Berresheim (2006) yields $1.4x10^{13}$ s/cm^3 because of the additional NO_x effects neglected in their derivation.

Approach (2) – budget of sources and sinks

All available and important sources and sinks listed in the following Table (S1) have been taken into account. Most of these were measured while H2 and methane were taken from former measurements (H_2) or atmospheric means (CH_4, 1.89 ppm_v).

OH sources	
$H_2O_2 + h\nu$	Measured: $J(H_2O_2)$, H_2O_2
$HONO + h\nu$	Measured: J(HONO), HONO
$HNO_3 + h\nu$	Measured: $J(HNO_3)$, HNO_3
$O(^1D) + h\nu$	Meas.: $J(O^1D)$, Approx..: steady-state app. (O^1D (meas.: O_3, H_2O, J))
$HO_2 + NO$	Meas.: NO, approx.: steady-state app. (HO_2) $k(HO_2+NO)$: MCMv3
$HO_2 + NO_3$	Meas.: NO_3, approx.: steady-state app. (HO_2) $k(HO_2+NO_3)$: MCMv3
$HO_2 + O_3$	Meas.: O_3, Approx.: steady-state app. (HO_2) $k(HO_2+NO_3)$: MCMv3

OH sinks	
+ CO	Meas.: CO k(OH+CO): MCMv3
+ CH_4	Approx.: CH_4 = 1.89 ppm_v k(OH+CH_4): MCMv3
+ O_3	Meas.: O_3 k(OH+O_3): MCMv3
+ NO	Meas.: NO k(OH+NO): MCMv3
+ NO_3	Meas.: NO_3 k(OH+NO_3): MCMv3
+ HONO	Meas.: HONO k(OH+HONO): MCMv3
+ HO_2NO_2	Approx.: steady-state-app. (HO_2NO_2) k(OH+HO_2NO_2): MCMv3
+ HNO_3	Approx..: (HNO_3) k(OH+HNO_3): MCMv3
+ HO_2	Approx.: steady-state app. (HO_2) k(OH+HO_2): MCMv3
+ H_2	Approx.: former meas. (H_2, T. Keber) k(OH+H_2): MCMv3
+ NO_2	Meas.: NO_2 k(OH+NO_2): MCMv3
+ H_2O_2	Meas.: H_2O_2 k(OH+H_2O_2): MCMv3
+ VOCs (methanol, acetaldehyde, acetone, isoprene, monoterpenes, nopinone/sabinaket.,linalool, pinonaldehyde/limonaket., sesquiterpenes	Meas.: VOCs (PTR-MS) k(OH+VOC): MCMv3 or Bourtsoukidis et al. (2012) for MT- and SQT-mixtures
+ HCHO	Meas.: HCHO (dual enzyme, aero laser) k(OH+HCHO): MCMv3

Table S1: Budget terms considered and input (measurement or approximation)

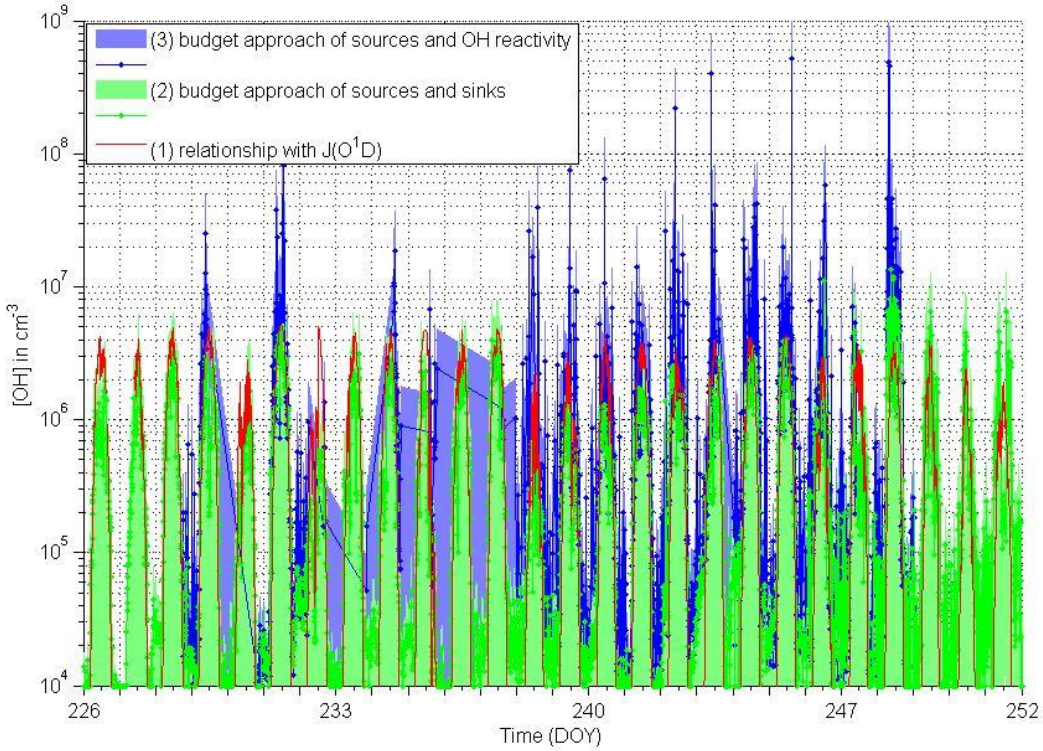

Figure S6. Extended results of all different approaches (1), (2) and (3) shown in Fig 3 of the study.

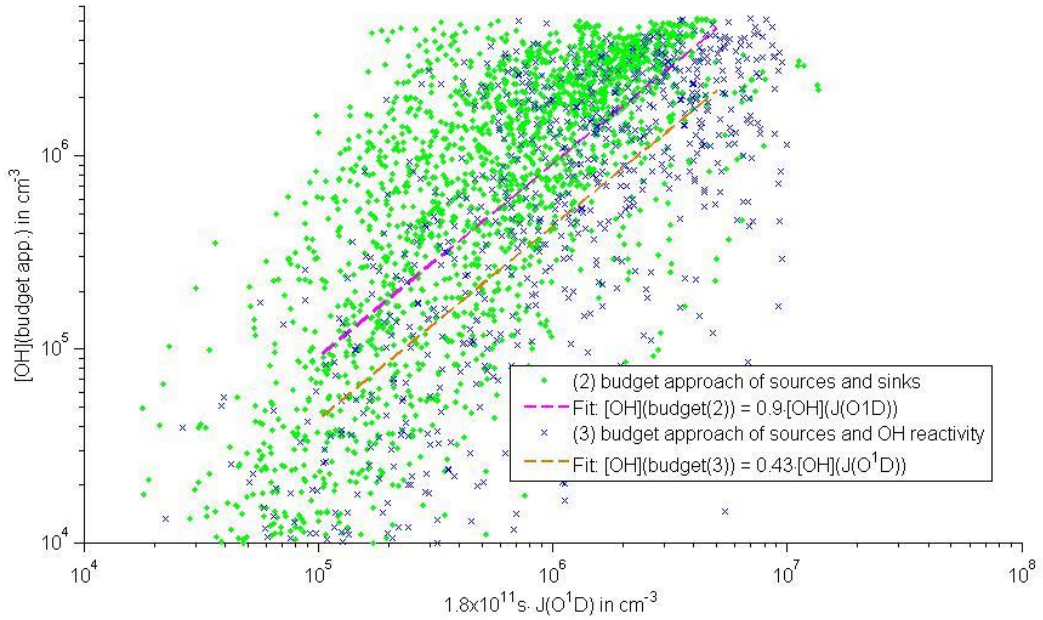

Figure S7. Scatter plot of approach (1) vs. approaches (2) and (3) with fits.

C) Correlation of $J(O^1D)$ and OH

As provided by Rohrer and Berresheim (2006) there is a clear link between the ambient hydroxyl radical OH concentration and the photolysis rate of O^1D. Therefore measured J(O1D) values and calculated [OH] ones using the general equations provided by Rohrer & Berresheim (2006) are plotted in Figure S8. Using this, a clear dependency was found for Mt. Kleiner Feldberg:

$$[OH] = (1.8 \pm 0.1) \times 10^{11} s^{-1} \cdot J(O^1D)$$

The slope is smaller than the one observed for Jungfraujoch (D) indicating a notable pollution impact.

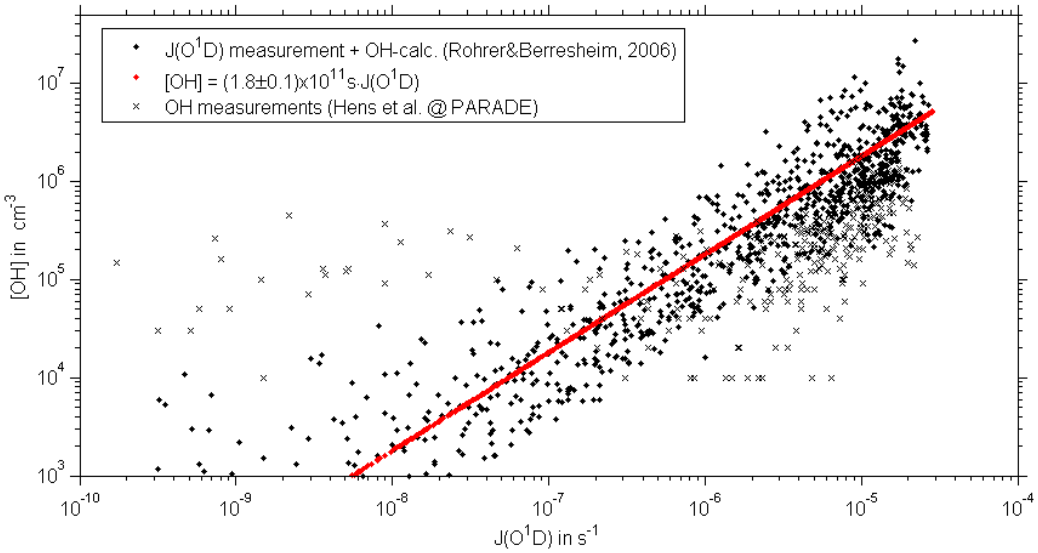

Figure S8. Scatter plot of the photolysis rate of O1D ($J(O^1D)$) and the measured OH concentration.

D) Mean daily intercomparison of individual hypotheses (A), (B) and (C)

This next section intercompares the mean daily behaviour of measured particle formation rate at 3 nm in particle diameter and the corresponding hypotheses (A), (B) and (C) as described in the paper.

Please consider the following for the Figure presented:

- Only available data were used for the intercomparison. This is reduced for sulfuric acid related ones because of the smaller measurement dataset.
- Lower uncertainty values were partially set to small values where mean deviations exceeded the mean values to facilitate a logarithmic plotting.

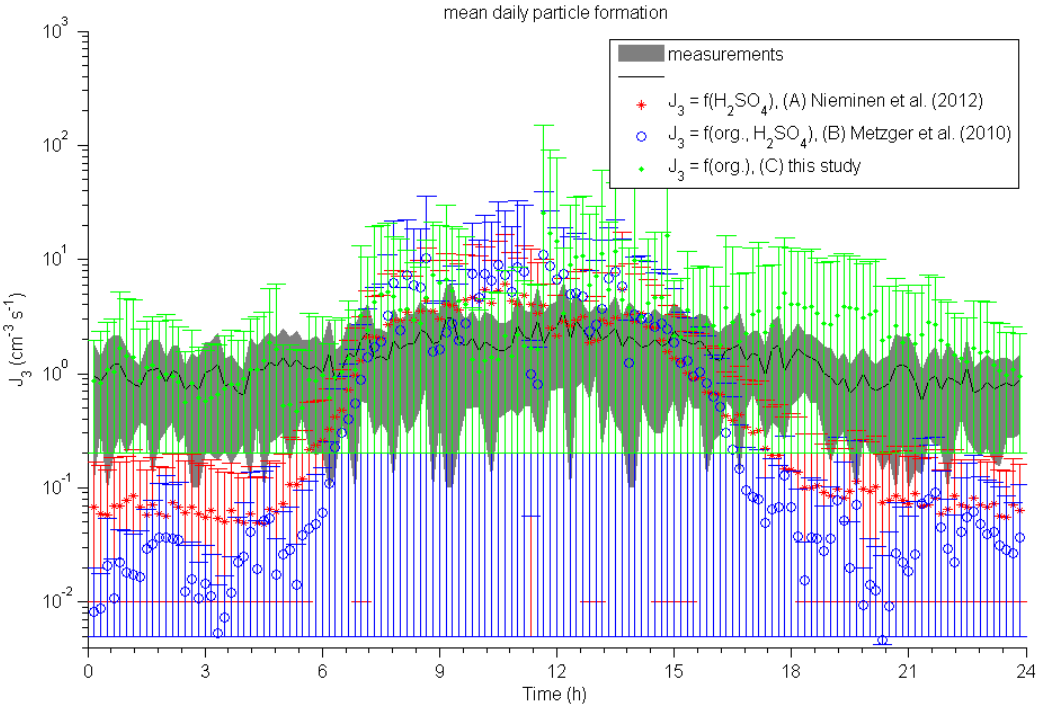

Figure S9. Mean daily pattern of measured and calculated particle formation rates at 3 nm in diameter.

E) Mean daily intercomparison of stepwise transfer from (C) to (B)

Here we transfer from approach (C) (organic only) to approach (B) (mixed) in the following manner: Step 1 – fixing the concentration of nucleation initiation molecules (or stable clusters), i.e. the secondary ozonide molecules to (4.6±3.6)x10^6 molecules cm^{-3}. Step 2 – additionally replacing the calculated RO_2 from terpene oxidation to a steady-state approach k_{MT}^{OH}*[MT][OH]/CS. Step 3 – finally skipping the minimum function and the inclusion of stabilized Criegee intermediate limitation.

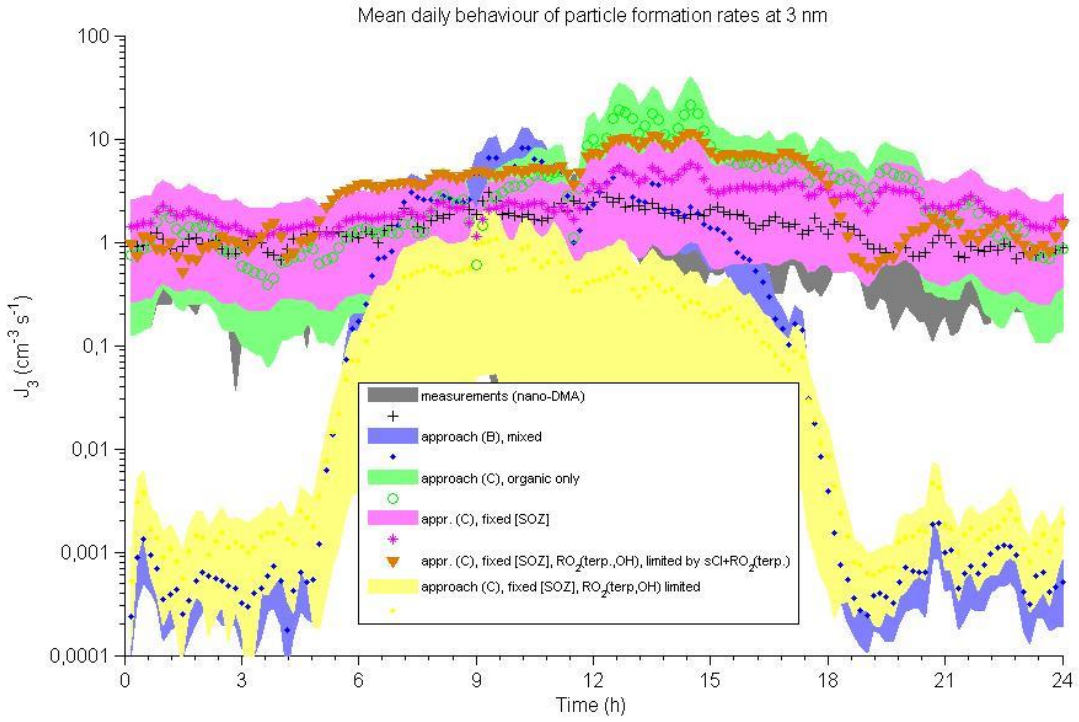

Figure S10. Mean daily pattern of measured and calculated particle formation rates at 3 nm in diameter transfering stepwise from approach (C) to (B).

The figure clearly indicates that the limitation to OH as nucleating species is causing the notable deviations of approaches (A) and (B) from the measured values. Approach (B) is somewhat worse than approach (A) during this campaign due to its fixation to a linear sulfuric acid dependency. However, this is environment and therefore site specific.

F) Individual linear regression of compounds with the particle formation rate J_3

As described in the article linear regressions of the particle formation rate at 3 nm were investigated for the following compounds: H_2SO_4, RO_2(C>5), OH, sCI, NO_3, HO_2, SOZ and NO. They were treated in this way:

$$J_3 = A \cdot [compound] + B$$

The relationships found are provided in the following Table S2.

Table S2. Linear regression factors for compounds with the particle formation rate at 3 nm in particle diameter.

Compound	***A [s^{-1}]***	***B [cm^{-3} s^{-1}]***
H_2SO_4 (meas.)	$(3.6\pm0.3)\times10^{-7}$	0.98±0.04
RO_2(C>5) (calc.)	$(9.1\pm1.1)\times10^{-9}$	1.01±0.04
OH (meas.+calc.)	$(1.76\pm0.09)\times10^{-6}$	1.02±0.04
OH (meas.)	$(1.3\pm0.3)\times10^{-6}$	1.0±0.1
sCI (calc.)	$(9.3\pm7.5)\times10^{-8}$	1.27±0.05
NO_3 (meas.)	$(1.3\pm0.5)\times10^{-10}$	0.99±0.4
HO_2 (meas.)	$(8.3\pm1.6)\times10^{-9}$	0.41±0.13
SOZ (calc.)	$(9.0\pm0.7)\times10^{-8}$	0.82±0.07
NO (meas.)	$(5.3\pm0.3)\times10^{-11}$	1.08±0.03